Chinese Chemical Letters 33 (2022) 3842–3848

Contents lists available at ScienceDirect

Chinese Chemical Letters

journal homepage: www.elsevier.com/locate/cclet

Anisotropic black phosphorene nanotube anodes afford ultrafast kinetic rate or extra capacities for Li-ion batteries

Huili Wang[a], Qian Gao[b], Cheng Liu[a], Yu Cao[a], Shuo Liu[a], Baoshan Zhang[a], Zhenpeng Hu[b,*], Jie Sun[a,*]

[a] Key Laboratory for Green Chemical Technology of Ministry of Education, School of Chemical Engineering and Technology, Tianjin University, Tianjin 300072, China
[b] School of Physics, Nankai University, Tianjin 300071, China

ARTICLE INFO

Article history:
Received 25 September 2021
Revised 3 November 2021
Accepted 7 November 2021
Available online 12 November 2021

Keywords:
Black phosphorene nanotubes
Lithium-ion battery
Anode materials
Li-storage performance
First principles calculations

ABSTRACT

As an important anode material for fast-charging Li-ion batteries (LIBs), black phosphorus (BP) has attracted extensive attention. Black phosphorene nanotubes (BPNTs) can be theoretically produced by rolling up the black phosphorene nanosheet along armchair (a-BPNTs) and zigzag (z-BPNTs) directions. The effects of curvature, chirality, Li-storage concentrations and strain stress on the Li-storage performance such as Li diffusion barriers and mechanical stabilities of BPNTs are mainly investigated by first principles calculations. The theoretical calculations predict that the a-BPNTs and z-BPNTs have good maximum Li-storage capacities, and the z-BPNTs exhibit better flexibility than a-BPNTs. The mechanical stabilities and Li-migration are all related to the curvature of BPNTs. Additionally, both a-BPNTs and z-BPNTs exhibit fast Li-ion conductivity along the *c*-axis direction. Moreover, the average Poisson's ratio of a-BPNTs (0.68) is larger than that of z-BPNTs (0.17), indicating that the strain stress is more difficult to apply on a-BPNTs than z-BPNTs. Our calculations predict that the a-BPNTs can afford ultrafast kinetic rate for fast-charging and high-power LIBs, while the z-BPNTs can provide extra capacity for high-energy LIBs.

Black phosphorus (BP), owning the most thermodynamically stable structure among the allotropes of phosphorus, was rediscovered as a member of two dimensional (2D) layered materials in 2014 [1,2]. Due to the anisotropy of BP structure, BP possesses unique anisotropic mechanical, phononic, optical, electronic and ion transport properties [3–8]. Studies have also found that black phosphorus has tunable band gap, carrier mobility and magnetic properties *via* changing the number of layers, in-plane strain, vacancies or adatoms, *etc.* [9–12]. Based on the unique characteristics, BP shows great potential in various applications, such as batteries, supercapacitors, field-effect transistors, diodes and phototransistors [13–19].

As the anode for Li-ion battery, BP possesses high theoretical capacity (2596 mAh/g), good Li-ion conductivity and relatively low, yet safe lithiation potential (0.7 V *versus* Li^+/Li), which can improve the high-rate performance and inhibit the formation of dendrites at overcharging and fast-charge conditions, respectively [8,20-22]. Han *et al.* predicted that bulk BP can only provide a specific capacity of 164.4 mAh/g ($Li_{0.19}P$) [23]. Kuo *et al.* suggested the specific capacities of monolayer and bilayer BP were 216.3 mAh/g ($Li_{0.25}P$) and 432.7 mAh/g ($Li_{0.5}P$), respectively [24]. Alternatively, studies asserted that the specific capacity of monolayer BP was 432.7 mAh/g ($Li_{0.5}P$) [25,26]. However, the BP structures discussed above are all 2D flat configurations, and the layered BP exhibits huge volumetric expansion (~300%) during lithiation process which leads to the deterioration of its cycling stability, limiting its application. In order to improve the capacity and cycling stability, various strategies have been adopted, such as nanoparticle composites with carbon, p-type doping, heterostructures [27,28]. Despite these efforts, these electrodes still suffer from rapid capacity fading during charge-discharge cycling. Nowadays, many nanotubes have been synthesized from 2D layered materials and studies found that the nanotubes offer superior electronic and mechanical performance [29–31]. For example, silicon nanotubes show better cycling stability than solid structures in energy storage equipment, as the nanotubes can increase the surface area accessible to the electrolyte and hollow structures can provide buffer space for volume expansion [32,33]. Similar to graphite and silicon, BP can be easily exfoliated to single-/few-layer structures through physical or chemical method [34,35]. Although no one has reported the synthesis of black phosphorene nanotubes (BPNTs) at present, theoret-

* Corresponding authors.
E-mail addresses: zphu@nankai.edu.cn (Z. Hu), jies@tju.edu.cn (J. Sun).

https://doi.org/10.1016/j.cclet.2021.11.030
1001-8417/

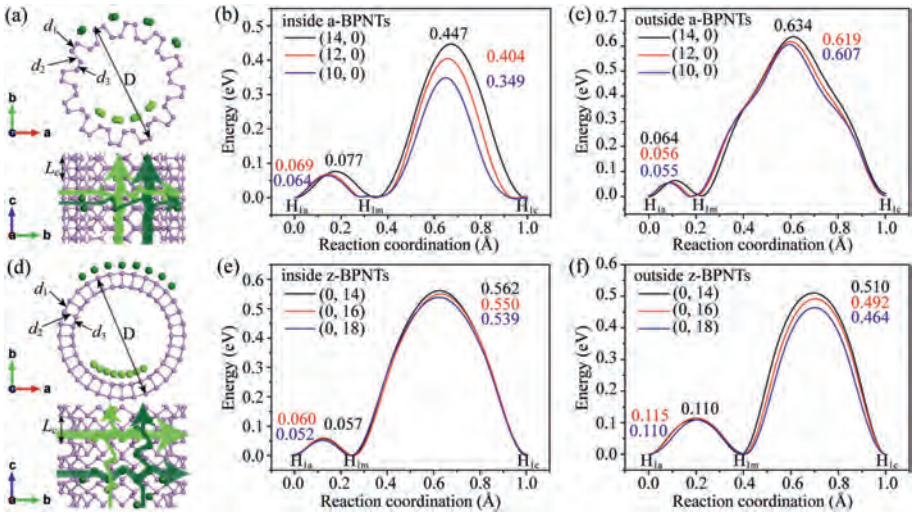

Fig. 1. The top view and side view of (a) a-BPNTs and (d) z-BPNTs, and corresponding migration trajectories of some Li atoms on the surface. The energy barriers for Li diffusion on (b, c) a-BPNTs and (e, f) z-BPNTs with different diameters.

ical calculations predicted that BPNTs can be stable [36–39]. Thus, it is necessary to investigate the Li-storage performance of BPNTs to provide theoretical guidance for the experiment.

BP affords a superior Li-ion conductivity along zigzag direction and a good electronic conductivity along armchair direction due to its structural anisotropy [7,8]. Herein, two kinds of BPNTs are taken into account in the present work by rolling up the BP nanosheet along armchair (a-BPNTs) and zigzag (z-BPNTs) directions, respectively. The effects of curvature, Li-storage concentrations and strain stress on the Li-storage performance are mainly investigated by first principles calculations. All the calculations are performed by the VASP code, with the generalized gradient approximation (GGA) of Perdew, Burke, and Ernzerhof (PBE) to describe the exchange correlation potential [40,41]. A plane-wave cutoff of 400 eV is used and the energy and Hellmann-Feynman force convergence criteria for electronic and ionic interaction are set at 10^{-5} eV and 0.03 eV/Å, respectively. The van der Waals (vdW) correction is included using optB86b-vdW functional in our calculations [42]. A $3 \times 4 \times 1$ supercell with 20 Å vacuum space is used to simulate the Li adsorption and diffusion on black phosphorene. To avoid the interaction between the nanotubes, the aperiodic length for a-BPNTs and z-BPNTs in the *a*/*b*-axial directions is set to 36 Å

The structural characteristics of a-BPNTs and z-BPNTs are firstly discussed. As shown in Fig. S1a (Supporting information), the lattice constants of the optimized black phosphorene are $a_1 = 4.50$ Å and $a_2 = 3.31$ Å in the armchair and zigzag directions, respectively, which are in agreement with the experimental and theoretical prediction [11,26,34]. The (n_1, n_2) BPNTs can be obtained by rolling up black phosphorene along the vector $\vec{R} = n_1\vec{a}_1 + n_2\vec{a}_2$, where n_1 and n_2 are the numbers of the unit cell along the two directions. In this study, we fabricated two kinds of BPNTs by rolling up monolayer BP along armchair (n_1, 0) (a-BPNTs) and zigzag (0, n_2) direction, respectively, as shown in Figs. 1a and d.

In order to investigate the effect of curvature on Li-storage performance, both a-BPNTs and z-BPNTs choose three simulation models with different diameters, (10/12/14, 0) and (0, 14/16/18) for a-BPNTs and z-BPNTs, respectively. The structural parameters of black phosphorene and BPNTs are listed in Table 1. The periodic unit-cell length (L_c) of BPNTs in the *c*-axial direction is obtained by fitting the energy with L_c using quadratic function as shown in Fig. S2 (Supporting information). It can be seen that the optimized unit-cell length L_c in the case of a-BPNTs is nearly the same with black phosphorene (3.31 Å, zigzag direction). Differently, the L_c of z-BPNTs shrinks, and the smaller radius exhibits the more obvious shrinkage compared with black phosphorene (4.50 Å, armchair direction). In addition, the unit-cell length L_c of z-BPNTs increases along with increasing diameters.

The strain energy, defined as the energy difference of per phosphorus atom between BPNTs and black phosphorene, is used to evaluate relative stabilities of BPNTs. The smaller strain energy predicts more stable structure. As shown in Table 1, the strain energy for both a-BPNTs and z-BPNTs decreases with the increase of diameters, indicating that BPNTs become more stable as the diameters increase. In addition, the stability of a-BPNTs is better than z-BPNTs when their diameters are similar, due to that the former possess lower strain energy which is in line with the results of Zeng *et al.* [37]. Bond length is another criterion to evaluate structural stability. As shown in Figs. 1a and d, d_1, d_2 and d_3 represent three types of P-P bonds and their lengths are listed in Table 1. In the case of black phosphorene, the longest bond is d_2 (~2.26 Å). In the case of a-BPNTs, the bond lengths of d_1, d_2 and d_3 are about 2.25 Å, 2.27 Å and 2.20 Å, respectively. Similar to black phosphorene, d_2 bond is the most unstable one for a-BPNTs, and is a little larger than that of black phosphorene. The average d_1 (~2.45 Å) in z-BPNTs is much larger than the average d_2 (~2.21 Å), d_3 (~2.18 Å), and the longest bonds in both a-BPNTs (d_2 ~2.27 Å) and black phosphorene (d_2 ~2.26 Å), respectively. In addition, the d_1 in z-BPNTs decreases with the increasing diameters, from 2.48 Å for (0, 14) to 2.42 Å for (0, 18), meaning an increasing stability. Considering the strain energy and the longest P-P bond, the a-BPNTs are more stable than z-BPNTs with the similar diameter, and the stability of both a-BPNTs and z-BPNTs increases with diameter.

The charge-discharge rate is a crucial indicator for rechargeable batteries which mainly depends on the migration speed of the intercalated metal-ions. To quantify this, it is essential to investigate the diffusion properties of Li atoms on black phosphorene and BPNTs [43]. The climbing image nudged elastic band method was performed to estimate the Li diffusion barrier [44]. The adsorption and diffusion of Li atoms on black phosphorene were firstly examined as shown and discussed in Fig. S1 (Supporting information). The results indicate that the Li atom will transfer to the nearest equivalent H_{1m} site no matter which direction it migrates along armchair (H_{1a}-H_{1b}) or zigzag (H_{1a}-H_{1c}) directions. The rate-limiting steps that Li diffusion along zigzag direction and armchair direction on black phosphorene are H_{1a}-H_{1m} and H_{1m}-H_{1c}, respectively, and the corresponding barriers are 0.074 eV and 0.603 eV, respectively.

Table 1
The diameter D, unit-cell length L_c in the axial direction, bandgap E_{gap}, the strain energy E_s, and P-P bond length d_1, d_2 and d_3.

BPNTs	D (Å)	L_c (Å)	E_{gap} (eV)	E_s (eV/atom)	d_1 (Å)	d_2 (Å)	d_3 (Å)
Black		3.31 (zigzag)	0.77	0	2.23	2.26	2.23
Phosphorene		4.50 (armchair)					
(10, 0)	17.14	3.31	0.29	0.05	2.25	2.27	2.19
(12, 0)	19.88	3.31	0.41	0.04	2.25	2.27	2.20
(14, 0)	22.71	3.31	0.50	0.03	2.25	2.27	2.20
(0, 14)	18.41	4.10	0.09	0.19	2.48	2.20	2.18
(0, 16)	20.43	4.16	0.16	0.15	2.45	2.21	2.18
(0, 18)	22.36	4.25	0.31	0.13	2.42	2.22	2.18

As the diffusion of alkali metal passing through the BP layer is very difficult [23], we first discussed the migration of Li adsorbed on the most stable adsorption H_1 site on the surface of a-BPNTs and z-BPNTs. To investigate the effect of curvature on Li diffusion, the diffusion barriers of Li on both a-BPNTs and z-BPNTs with three different diameters are calculated. According to the results discussed (Fig. S1), the periodic Li diffusion pathways on a-BPNTs along *c*-axis (zigzag) direction and perpendicularly to the *c*-axis (armchair) direction are H_{1a}-H_{1m}-H_{1b} and H_{1a}-H_{1m}-H_{1c}, respectively. The Li diffusion pathways on z-BPNTs along *c*-axis (armchair) direction and perpendicularly to the *c*-axis (zigzag) direction are H_{1a}-H_{1m}-H_{1c} and H_{1a}-H_{1m}-H_{1b} respectively. The Li diffusion along *c*-axis direction of a-BPNTs and z-BPNTs is first discussed which plays a key role in Li-ion conductivity of the nanotubes, and the corresponding rate-limiting steps are H_{1a}-H_{1m} and H_{1m}-H_{1c}, respectively. As shown in Figs. 1b and c, when Li migrates on a-BPNTs along the *c*-axis direction, the average barriers of Li migrating inside and outside the nanotubes are about 0.070 eV and 0.058 eV, respectively. The average barriers of Li migrating inside and outside z-BPNTs along the *c*-axis direction are 0.55 eV and 0.49 eV, respectively (Figs. 1e and f). Accordingly, Li migrates a little slower inside than outside the nanotubes along *c*-axis direction. As the barriers along *c*-axis directions of a-BPNTs and z-BPNTs decrease with decreasing diameters, the larger curvature of BPNTs, the faster diffusion of Li. For the first-layer Li, the a-BPNTs show better Li-ion conductivity along the *c*-axis direction than z-BPNTs. Moreover, the transmission of Li atoms perpendicularly to the *c*-axis of BPNTs is also considered. The average diffusion barriers of Li transports perpendicularly to the *c*-axis inside and outside a-BPNTs from H_{1m} to H_{1c} are 0.40 eV and 0.62 eV, respectively, indicating that the transport is difficult. Differently, the z-BPNTs show fast Li-ion conductivity perpendicularly to the *c*-axis direction as the average barriers of Li migrates inside and outside the nanotubes from H_{1a} to H_{1m} are only 0.06 eV and 0.11 eV, respectively.

According to the above analysis of the strain energy, the mechanical stability of a-BPNTs and z-BPNTs is strongly dependent on their curvature. In order to investigate the effect of curvature on the mechanical stability of lithiated BPNTs, the Li intercalation on a-BPNTs and z-BPNTs with different curvature is investigated. The Li-storage concentrations are another important factor affecting the structural stability and are crucial for practical applications in LIBs. Thus, the single-layer Li insertion at different concentrations are investigated by gradually increasing the number of Li atoms at the most energetically stable H_1 sites. The notation of Li_xP is used to represent the lithiated nanotubes with *x* representing the Li-intercalation concentration, which is equal to the ratio of Li atoms to P atoms. Two main Li-intercalation patterns, Li laying inside or outside the BPNTs, are also taken into account. The effect of strain energy on the structural stability of lithiated BPNTs is also studied by the change of unit-cell length L_c in the *c*-axis direction. The *c*-axis strain is defined as $\varepsilon_{c\text{-axis}} = (L_c - L_{c0})/L_{c0}$, where L_c and L_{c0} are the strained and relaxed unit-cell length of pristine a-BPNTs and z-BPNTs, respectively. The positive value ($\varepsilon_{c\text{-axi}} > 0$) means a tensile strain, and negative value ($\varepsilon_{c\text{-axi}} < 0$) corresponds to a compressive strain.

In the case of a-BPNT (10, 0) as shown in Fig. 2a, the structural stabilities of nanotubes with internal Li-intercalation are poor as the lithiated nanotubes can maintain stable structures with suitable unit-cell length L_c, but the structures are easy to broken into fragments under the action of *c*-axis strain stress. The lithiated a-BPNT (10, 0) can remain stable under the strain stress when the Li atoms are embedded outside nanotubes with low Li concentrations $x = 0.05$ and 0.125, while the nanotubes with high Li-concentration $x = 0.25$ are unstable coupled with the breaking of P-P bonds as shown in Fig. 2b. Whether Li atoms insert inside or outside the nanotubes, the lithiated a-BPNT (12, 0) can maintain stable structures under the strain stress, shown in Figs. 2c and d. Similarly, the lithiated a-BPNT (14, 0) also exhibit good structural stabilities under the strain stress (Figs. S3a and b in Supporting information). Therefore, it can be drawn that the a-BPNTs exhibit better Li-storage performance when their diameters are larger than that of a-BPNT (12, 0).

The effects of curvature, Li-storage concentrations and strain stress on the structural stability of z-BPNTs are also investigated. As shown in Fig. 3, when the Li concentration is low ($x \sim 0.05$), the shape of all lithiated z-BPNTs changes accompanied by the breaking of P-P bonds, but the nanotubes do not break into fragments under the strain stress. When the unit-cell length L_c is smaller than 4.55 Å, the z-BPNT (0, 14) with internal Li intercalation $x = 0.125$ can maintain the stable structures and the total energies decrease with the increasing unit-cell length L_c, while the nanotubes are destroyed coupled with the breaking of P-P bonds when the unit-cell length L_c is larger than 4.55 Å When the unit-cell length L_c is in the range of 3.80 Å to 4.80 Å, all the z-BPNTs (0, 14) with external Li intercalation $x = 0.125$ are destroyed. In comparison, the z-BPNTs (0, 16) with Li concentration $x = 0.125$ show good structural stabilities no matter Li atoms insert inside or outside the nanotubes. When the Li concentration is up to $x = 0.25$, the (0, 14) and (0, 16) with internal Li intercalation show good structural stabilities, while the nanotubes with external Li intercalation can remain the stable structures only at small tensile strain. Good structural stabilities are also observed in z-BPNT (0, 18) after Li intercalation as shown in Figs. S3c and d (Supporting information). Similarly, it can be also drawn that the z-BPNTs exhibit better Li-storage performance when their diameters are larger than that of z-BPNT (0, 16). As the diameters of a-BPNT (12, 0) and z-BPNT (0, 16) are all about 20 Å, we can get that the a-BPNTs and z-BPNTs show better Li-storage performance when their diameters are larger than 20 Å, that is, the curvature is less than 0.1.

The Li adsorption ability of Li_xP can be evaluated from their binding energy

$$E_b(\mathrm{x}) = \frac{1}{x}(E(Li_xP) - E(P) - xE(Li)) \quad (1)$$

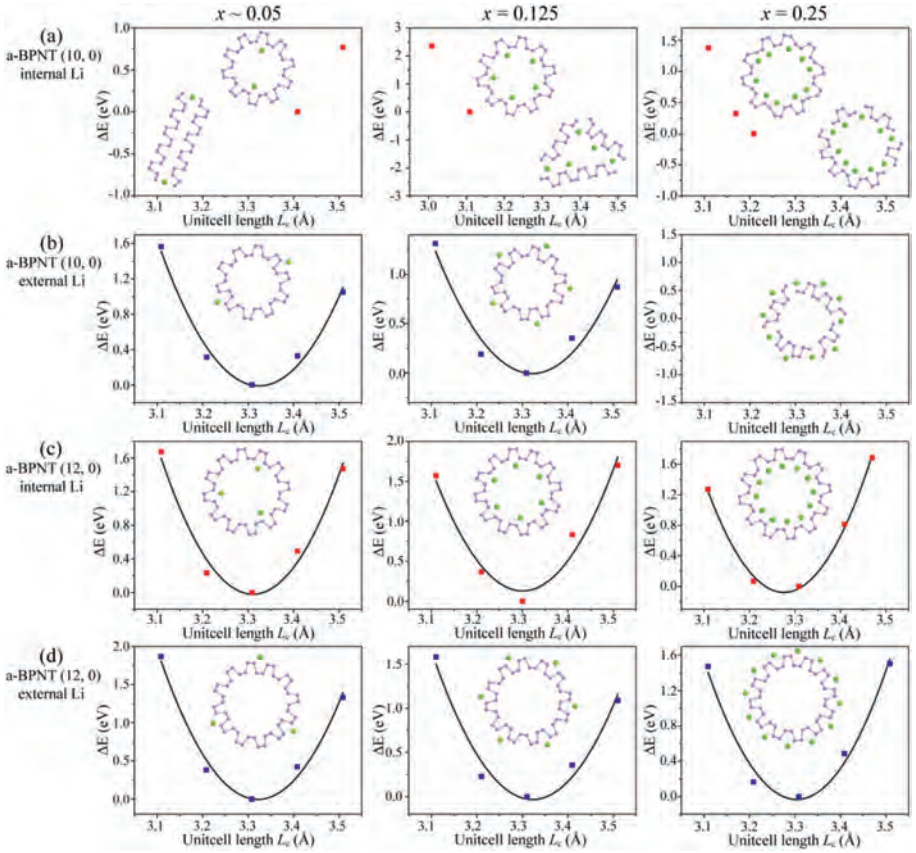

Fig. 2. Energy profiles of linear scans about the unit-cell length L_c along the *c*-axis for (a, b) a-BPNTs (10, 0) and (c, d) a-BPNTs (12, 0) with different internal or external Li-intercalation concentrations.

where $E(Li_xP)$ and $E(P)$ are total energies of lithiated and pristine BPNTs, respectively, $E(Li)$ is the average energy of per Li atom in the body-centered cubic (*bcc*) Li metal, and x is the Li concentration. The effect of curvature on the Li adsorption ability is discussed by comparing the binding energies with Li concentration $x = 0.125$ (Fig. S4 in Supporting information). The binding energies of a-BPNTs with external Li decrease slightly with the increasing diameters, indicating the gradually enhanced Li adsorption ability with decreasing curvature. However, the binding energies of a-BPNTs with internal Li intercalation and z-BPNTs with internal or external Li intercalation increase a little with increasing diameters, indicating the gradually weakened Li adsorption ability with decreasing curvature. In addition, the $E_b(x)$ of Li inserting to z-BPNTs is about 0.7 eV less than the corresponding $E_b(x)$ of Li inserting to a-BPNTs with similar diameters, indicating that Li atoms are more inclined to intercalate to z-BPNTs than a-BPNTs.

The unit-cell length L_c and diameters of pristine and lithiated a-BPNTs (12, 0) and z-BPNTs (0, 16) with the single-layer Li intercalation concentration less than $x = 0.25$ are summarized in Tables S1 and S2 (Supporting information), respectively. When the Li atoms insert inside the a-BPNT (12, 0), the L_c decreases a little while the diameter increases a little with the increasing Li concentrations. However, when the Li atoms insert outside the a-BPNT (12, 0), both the L_c and the diameter decrease a little with the increasing Li concentrations. In the case of z-BPNT (0, 16), the L_c and the diameters increases obviously after lithiation and can be affected evidently by the Li concentrations.

Electronic conductivity is another significant indicator of the electrode materials for rechargeable batteries. Fig. S5 (Supporting information) shows the total density of states of the lithiated a-BPNTs (12, 0) and z-BPNTs (0, 16) with different Li-intercalation concentrations. Similar to 2D BP [8], the lithiated a-BPNTs and z-BPNTs are converted from semiconductor to conductor with some electronic states distributed near the Fermi level, indicating an enhanced electronic conductivity.

Table 2
The Poisson ratio of pristine and lithiated a-BPNTs (12, 0) and z-BPNTs (0, 16).

BPNTs	Pristine	$x = 0.125$	
		Inside	Outside
(12, 0)	0.63	0.65	0.76
(0, 16)	0.23	0.13	0.16

Generally, a compression (or stretch) applied in an axial direction leads to an expansion (or compression) in the transverse direction. In the above, we define the *c*-axis strains $\varepsilon_{c\text{-axis}}$, and the corresponding transverse strain can be defined as $\varepsilon_{trans} = (D - D_0)/D_0$, where D and D_0 are the diameters of strained and relaxed BPNTs, respectively. Poisson's ratio (ν) is defined as the ratio between the *c*-axis strains $\varepsilon_{c\text{-axis}}$ and the corresponding transverse strain ε_{trans} as $\nu = -d\varepsilon_{trans}/d\varepsilon_{c\text{-axis}}$. Fig. S6 (Supporting information) displays the applied *c*-axis strain and their corresponding transverse strain of pristine and lithiated a-BPNT (12, 0) and z-BPNT (0, 16), and the Poisson's ratio is listed in Table 2. It can be seen that all the Poisson's ratios are positive and the Poisson's ratio of lithiated a-BPNT (12, 0) and z-BPNT (0, 16) with Li concentration $x = 0.125$ is nearly equal to that of corresponding pristine nanotubes. In addition, the Poisson's ratio of a-BPNT (12, 0) is larger than that of z-BPNT (0, 16) which means the strain stress is more difficult to apply on a-BPNT (12, 0) than z-BPNT (0, 16).

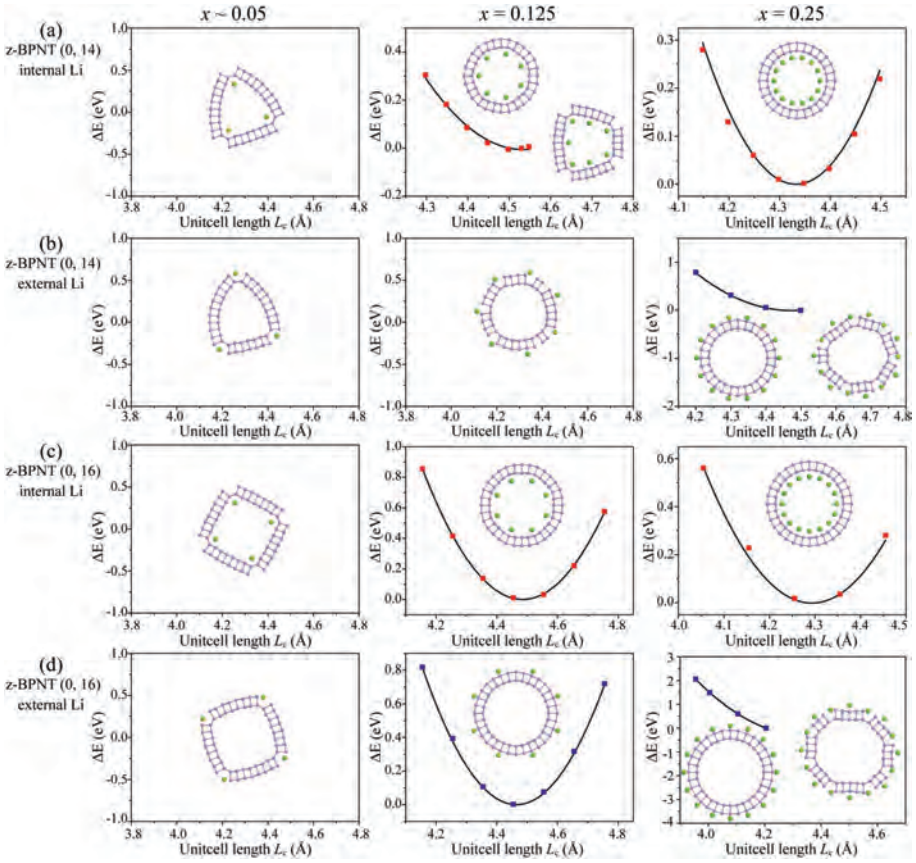

Fig. 3. Energy profiles of linear scans about the unit-cell length L_c along the *c*-axis for (a, b) z-BPNTs (0, 14) and (c, d) z-BPNTs (0, 16) with different internal or external Li-intercalation concentrations.

The above works have discussed the cases that only single-layer Li atoms are adsorbed on the internal or external wall of BPNTs. In practice, Li may exist inside and outside the BPNTs at the same time. The adsorption of Li with both internal and external intercalation for the stable a-BPNT (12, 0) and z-BPNT (0, 16) is investigated. As shown in Figs. S7a and b (Supporting information), the maximum Li concentration in a-BPNT (12, 0) is 0.375 with internal Li concentration $x = 0.25$ and external Li concentration $x = 0.125$, and the maximum Li concentration in z-BPNT (0, 16) is 0.625 with internal Li concentration $x = 0.375$ and external Li concentration $x = 0.25$. As shown in Fig. S7c (Supporting information), the maximum Li concentration of Li inserting outside the a-BPNT (12, 0) is 0.5, which is equal to that of Li inserting inside the nanotube. Therefore, compared with the single Li-intercalation method, the adsorption of Li in a-BPNTs with both internal and external intercalation is unfavorable for Li-storage. Interestingly, it shows different effects in z-BPNTs. The maximum Li concentrations of Li inserting inside or outside z-BPNTs using a single Li-intercalation method before the structural distortion are 0.375 and 0.25, respectively. Thus, the adsorption of Li in z-BPNTs with both internal and external intercalation can serve higher Li-storage capacity ($x = 0.625$) than using a single Li-intercalation method.

To verify whether the hollow structures of BPNTs are conducive to Li-storage and can inhibit the volume expansion, the properties of multilayer Li intercalation are discussed. As shown in Fig. 4a, when the Li-intercalation concentration of a-BPNT (12, 0) is up to $x = 0.5$, the Li atoms are uniformly distributed in the cavity, and the shape of the nanotube collapses a little with no broken P-P bonds. When the Li-intercalation concentration of a-BPNT (12, 0) is larger than $x = 0.5$, the tubular structures break into fragments with some overflowed Li atoms. In the case of z-BPNTs (0, 16)

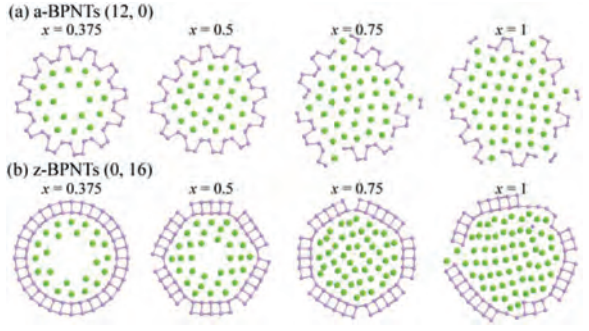

Fig. 4. Optimized structures for (a) a-BPNTs (12, 0) and (b) z-BPNTs (0, 16) with different internal Li-intercalation concentrations.

shown in Fig. 4b, when the Li-intercalation concentrations is up to $x = 0.75$, the tubular structures can keep well even if some P-P bonds break, while the nanotube was destroyed when the Li-concentration is up to $x = 1$.

The Li-storage capacity C (mAh/g) can be computed as follows:

$$C = \frac{1}{3.6M_P}[x \times z \times F] \quad (2)$$

where x is the Li concentration, z is the valence number ($z = 1$ for Li), F is Faraday constant (96,485 C/mol), and M_P is the atomic mass of P (30.97 g/mol). According to the definition, the theoretical capacities of a-BPNT (12, 0) and z-BPNT (0, 16) are 432.7 mAh/g ($Li_{0.5}P$) and 649.0 mAh/g ($Li_{0.75}P$), respectively. Compared with the Li-storage capacity of bulk BP (164.4 mAh/g), it can be seen that

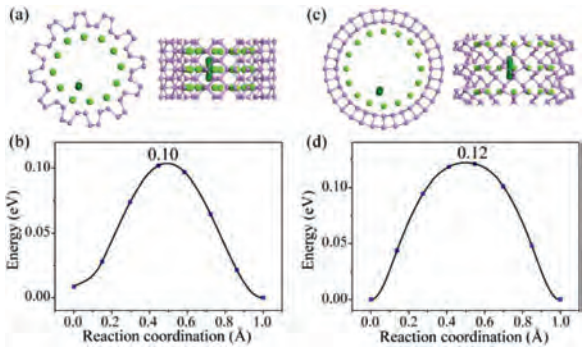

Fig. 5. The diffusion pathways and energy barriers for Li diffusion on (a, b) a-BPNT (12, 0) and (c, d) z-BPNT (0, 16) along *c*-axis direction.

the Li-storage performance can also be enhanced by rolling the BP nanosheet into nanotubes.

The Li intercalation voltage is also calculated to explore the electrochemical performance of BPNTs. Usually the effects of entropy and volume are negligible during the reaction. The average voltage (V_{avg}) of lithiated BPNTs defined as Li_xP with Li concentration in the range of $x_1 < x \leq x_2$ can be determined by:

$$V_{avg} = \frac{E_{(Li_{x1}P)} - E_{(Li_{x2}P)} + (x_2 - x_1)E_{(Li)}}{(x_2 - x_1)e} \quad (3)$$

where $E_{(Li_{x1}P)}$, $E_{(Li_{x2}P)}$ and $E_{(Li)}$ are the energy of $Li_{x1}P$, $Li_{x2}P$ and a single Li atom, respectively. According to the definition, the average voltages of a-BPNT (12, 0) and z-BPNT (0, 16) with external Li intercalation ($0 < x \leq 0.25$) are 1.94 V and 2.58 V, respectively. The Li storage inside the BPNTs is divided into two steps: single-layer Li intercalation and multilayer Li intercalation. Based on this, the average voltages of a-BPNT (12, 0) with the Li concentration in the range of $0 < x \leq 0.25$ and $0.25 < x \leq 0.5$ are 2.15 V and 2.04 V, respectively. In addition, the average voltages of z-BPNT (0, 16) with the Li concentration in the range of $0 < x \leq 0.25$ and $0.25 < x \leq 0.75$ are 2.31 V and 1.93 V, respectively. Studies found that the average voltage of monolayer BP is 2.9 V ($0 \leq x \leq 0.25$) [8], which is much higher than that of BPNTs. Hence, we can draw the conclusion that the BPNTs possess lower average voltage than monolayer BP.

In the case of Li-intercalation concentration $x = 0.375$ as shown in Fig. 4, the Li atoms are dispersed into two layers. The structural parameters of a-BPNT (12, 0) and z-BPNT (0, 16) with Li-intercalation concentration $x = 0.25$ and 0.375 are shown in Table S3 (Supoprting information). Interestingly, the tubular structures of both a-BPNT (12, 0) and z-BPNT (0, 16) with Li-intercalation concentration $x = 0.375$ not only remain well but also have decreased diameters compared with corresponding that with Li-intercalation concentration $x = 0.25$. The migration of the second-layer Li is also considered. The migration pathways along the *c*-axis direction are selected and the optimized pathways are shown in Fig. 5. The calculated diffusion barriers for the second-layer Li along the *c*-axis direction of a-BPNT (12, 0) and z-BPNT (0, 16) are 0.10 eV and 0.12 eV, respectively. These results indicate that the intercalation of the Li atoms in the second layer not only is beneficial to maintain the structural stability but also provides new Li transport channels. Compared with other anode materials, such as graphene (0.28 eV) [45], silicon (0.23 eV) [46] and MoS_2 (0.21 eV) [47], the a-BPNTs (0.07 eV) and z-BPNTs (0.12 eV) exhibit super high Li-ion conductivity along the *c*-axis direction.

In summary, the effect of curvature, chirality and strain stress on the Li-storage performance and mechanical stability of a-BPNTs and z-BPNTs were investigated by first principles calculations. Our calculations show that the cavity structures of both a-BPNTs and z-BPNTs are conducive to Li-storage, and the maximum Li-storage capacities of a-BPNTs and z-BPNTs are 432.7 mAh/g and 649.0 mAh/g, respectively. The curvature plays a key role in mechanical stabilities and Li-ion conductivity for both a-BPNTs and z-BPNTs. The lithiated nanotubes can maintain tubular structures well under the condition of *c*-axis strain tress when their curvature is less than ~0.1. Furthermore, the larger curvature of BPNTs, the more conducive to the migration of lithium ions along the *c*-axis direction, especially the transmission of Li laying outside the a-BPNTs and z-BPNTs. The diffusion barrier of first-layer Li along *c*-axis direction on a-BPNTs (0.06 eV) is about one-tenth of that on z-BPNTs (0.52 eV), while the difference between the diffusion barriers of the second-layer Li on a-BPNTs (0.10 eV) and z-BPNTs (0.12 eV) along *c*-axis direction is very small. Moreover, the pristine and lithiated a-BPNTs and z-BPNTs all have positive Poisson's ratios, and the average Poisson's ratio of a-BPNTs (0.68) is larger than that of z-BPNTs (0.17). Our results predict that both the a-BPNTs and z-BPNTs can serve as good anode materials for high-power LIBs.

Declaration of competing interest

The authors declare that they have no known competing financial interests or personal relationships that could have appeared to influence the work reported in this paper.

Acknowledgments

This work was supported by the National Key Research and Development Program of China (No. 2019YFE0118800), National Natural Science Foundation of China (Nos. 22005215, 21773124) Tianjin Science and Technology Project (No. 19YFSLQY00070) and Hebei Province Innovation Ability Promotion Project (Nos. 20544401D, 20312201D).

Supplementary materials

Supplementary material associated with this article can be found, in the online version, at doi:10.1016/j.cclet.2021.11.030.

References

[1] L.K. Li, Y.J. Yu, G.J. Ye, et al., Nat. Nanotechnol. 9 (2014) 372–377.
[2] M. Buscema, D.J. Groenendijk, S.I. Blanter, et al., Nano Lett. 14 (2014) 3347–3352.
[3] Y.Q. Cai, Q.Q. Ke, G. Zhang, et al., Adv. Funct. Mater 25 (2015) 2230–2236.
[4] H. Jang, J.D. Wood, C.R. Ryder, M.C. Hersam, D.G. Cahill, Adv. Mater. 27 (2015) 8017–8022.
[5] L. Henry, V. Svitlyk, M. Mezouar, et al., Nanoscale 12 (2020) 4491–4497.
[6] W. Zheng, A. Nemilentsau, D. Lattery, et al., Adv. Opt. Mater. 6 (2018) 1–9.
[7] J.Q. He, D.W. He, Y.S. Wang, et al., ACS Nano 9 (2015) 6436–6442.
[8] W.F. Li, Y.M. Yang, G. Zhang, Y.W. Zhang, Nano Lett. 15 (2015) 1691–1697.
[9] J.S. Qiao, X.H. Kong, Z.X. Hu, F. Yang, W. Ji, Nat. Commun. 5 (2014) 1–7.
[10] X.Y. Han, H.M. Stewart, S.A. Shevlin, C.R.A. Catlow, Z.X. Guo, Nano Lett. 14 (2014) 4607–4614.
[11] P. Srivastava, K.P.S.S. Hembram, H. Mizuseki, et al., J. Phys. Chem. C 119 (2015) 6530–6538.
[12] J. Kim, S.S. Baik, S.H. Ryu, et al., Science 349 (2015) 723–726.
[13] C. Liu, X.P. Han, Y. Cao, et al., Energy Stor. Mater. 20 (2019) 343–372.
[14] C. Liu, Y.H. Wang, J. Sun, A.B. Chen, Trans. Tianjin Univ. 26 (2020) 104–126.
[15] J. Sun, H.W. Lee, M. Pasta, et al., Nat. Nanotechnol. 10 (2015) 980–985.
[16] D.D. Liu, Y.L. Shi, Li Tao, et al., Chin. Chem. Lett. 30 (2019) 207–210.
[17] H. Huang, H.H. Wu, C. Chi, et al., J. Mater. Chem. A 7 (2019) 8897–8904.
[18] B.L. Xu, S.H. Qi, M.M. Jin, et al., Chin. Chem. Lett. 30 (2019) 2053–2064.
[19] Y.L. Yang, M.G. Wu, X.Q. Zhu, et al., Chin. Chem. Lett. 30 (2019) 2065–2088.
[20] J. Sun, G.Y. Zheng, H.W. Lee, et al., Nano Lett. 14 (2014) 4573–4580.
[21] H.C. Jin, S. Xin, C.H. Chuang, et al., Science 370 (2020) 192–197.
[22] C. Liu, M.Y. Han, Y. Cao, et al., Energy Stor. Mater. 37 (2021) 417–423.
[23] K.P.S.S. Hembram, H. Jung, B.C. Yeo, et al., Phys. Chem. Chem. Phys. 18 (2016) 21391–21397.
[24] Q.F. Li, C.C. Duan, X.G. Wan, J.L. Kuo, J. Phys. Chem. C 119 (2015) 8662–8670.
[25] S.J. Zhao, W. Kang, J.M. Xue, J. Mater. Chem. A 2 (2014) 19046–19052.
[26] J. Cao, J. Shi, Y.Q. Hu, et al., Appl. Surf. Sci. 392 (2017) 88–94.
[27] X.P. Han, J.P. Han, C. Liu, J. Sun, Adv. Funct. Mater. 28 (2018) 1–56.
[28] H. Huang, Y.W. Yang, J.M. Zhu, et al., Appl. Surf. Sci. 561 (2021) 150093.

[29] Z.Q. Wang, D. Wang, Z.Y. Zou, et al., Natl. Sci. Rev. 7 (2020) 1768–1775.
[30] L. Li, J.P. Deng, Y.C. Gou, et al., Carbon 18 (2021) 721–734.
[31] Q. Gao, S.L. Hu, Y. Du, Z.P. Hu, J. Mater. Chem. A 5 (2017) 4827–4834.
[32] M.H. Park, M.G. Kim, J. Joo, et al., Nano Lett. 9 (2009) 3844–3847.
[33] H. Wu, G. Chan, J.W. Choi, et al., Nat. Nanotechnol. 7 (2012) 310–315.
[34] Z.H. Wu, Y.X. Lyu, Y. Zhang, et al., Nat. Mater. 20 (2021) 1203–1209.
[35] L. Li, D. Zhang, J.P. Deng, Y.C. Gou, J.F. Feng, J. Energy Chem. 49 (2020) 365–374.
[36] L.X. Guan, G.F. Chen, J.G. Tao, Phys. Chem. Chem. Phys. 18 (2016) 15177.
[37] H.Y. Guo, N. Lu, J. Dai, et al., J. Phys. Chem. C 118 (2014) 14051–14059.
[38] L. Wang, C. Wang, Phys. Chem. Chem. Phys. 20 (2018) 28726–28731.
[39] Q.F. Li, H.F. Wang, C.H. Yang, et al., Appl. Surf. Sci. 441 (2018) 1079–1085.
[40] G. Kresse, J. Furthmüller, Comput. Mater. Sci. 6 (1996) 15–50.
[41] J.P. Perdew, K. Burke, M. Ernzerhof, Phys. Rev. Lett. 77 (1996) 3865.
[42] J. Klimeš, D.R. Bowler, A. Michaelides, J. Phys. 22 (2010) 022201.
[43] S.Q. Shi, J. Gao, Y. Liu, et al., Chin. Phys. B 25 (2016) 018212.
[44] G. Henkelman, B.P. Uberuaga, H.J. Jónsson, Chem. Phys. 113 (2000) 9901–9904.
[45] L.J. Zhou, Z.F. Hou, L.M. Wu, J. Phys. Chem. C 116 (2012) 21780–21787.
[46] G.A. Tritsaris, E. Kaxiras, S. Meng, E. Wang, Nano Lett. 13 (2013) 2258–2263.
[47] Y.F. Li, D.H. Wu, Z. Zhou, et al., J. Phys. Chem. Lett. 3 (2012) 2221–2227.